

Title:

Individual correspondence of amyloid- β and intrinsic connectivity in the posterior default mode network across stages of Alzheimer's disease

Authors/Affiliation:

Lorenzo Pasquini *^{†1,9}, Gloria Benson ^{†5,9}, Michel J. Grothe ⁶, Lukas Utz ^{4,9}, Nicholas E. Myers ^{7,9}, Igor Yakushev ^{3,9}, Timo Grimmer ^{2,9}, Martin Scherr ^{2,8,9}, Christian Sorg ^{2,4,9} for the Alzheimer's Disease Neuroimaging Initiative⁺.

¹Memory and Aging Center, Department of Neurology, University of California at San Francisco, 675 Nelson Rising Lane, 94158 San Francisco, USA; Departments of ² Psychiatry and Psychotherapy, ³ Nuclear Medicine, and ⁴ Neuroradiology of Klinikum rechts der Isar, Technische Universität München, Ismaninger Straße. 22, 81675 Munich, Germany; ⁵ Department of Neurology and NeuroCure Clinical Research Center, Charité Universitätsmedizin, Charitéplatz 1, 10117 Berlin, Germany; ⁶ German Center for Neurodegenerative Diseases (DZNE), Gehlsheimer Str. 20, 18147 Rostock, Germany; ⁷ Oxford University, Department of Experimental Psychology, 9 South Parks Road, Oxford OX1 3UD, United Kingdom; ⁸ Department of Neurology, Christian Doppler

Klinik, Paracelsus Medical University Salzburg, Salzburg, Austria;

⁹TUM-Neuroimaging Center, Technische Universität München,
Ismaninger Straße 22, 81675 Munich, Germany.

†These authors contributed equally to this work

⁺Data used in preparation of this article were obtained from the Alzheimer's Disease Neuroimaging Initiative (ADNI) database (adni.loni.usc.edu). As such, the investigators within the ADNI contributed to the design and implementation of ADNI and/or provided data but did not participate in analysis or writing of this report. A complete listing of ADNI investigators can be found at: http://adni.loni.usc.edu/wp-content/uploads/how_to_apply/ADNI_Acknowledgement_List.pdf

Running title:

A β and connectivity correspondence in AD

Corresponding author:

Lorenzo Pasquini, Memory and Aging Center, Department of Neurology, University of California at San Francisco, 675 Nelson Rising Lane, 94158 San Francisco, USA, Phone: +1 415 502 7187, email: lorenzo.pasquini@ucsf.edu

Abstract:

In Alzheimer's disease (AD), amyloid- β ($A\beta$) pathology and intrinsic functional connectivity (iFC) interact. Across stages of AD, we expected individual spatial correspondence of $A\beta$ and iFC to reveal both $A\beta$ accumulation and its detrimental effects on iFC. We used resting-state functional magnetic imaging and $A\beta$ imaging in a cross-sectional sample of 90 subjects across stages of AD and healthy older adults. Global and local correspondence of $A\beta$ and iFC were assessed within the posterior default mode network (pDMN) by within-subject voxel-wise correlations. Beginning at preclinical stages, global $A\beta$ -iFC correspondence was positive for the whole pDMN—showing that $A\beta$ accumulates in areas of high connectivity— and reached a plateau at prodromal stages. Starting at preclinical stages, local correspondence was negative in network centers—indicating that $A\beta$ reduces connectivity of the pDMN as a function of local plaque concentration—and peaked at prodromal stages. Positive global correspondence suggests that $A\beta$ accumulation progresses along iFC, with this effect starting in preclinical stages, and being constant along clinical periods. Negative local correspondence suggests detrimental effects of $A\beta$ on iFC in network centers, starting at preclinical stages, and peaking when first symptoms appear. Data reveal a complex trajectory of $A\beta$ and iFC

correspondence, affecting both A β accumulation and iFC impairments.

Key words:

Alzheimer's disease; amyloid- β ; intrinsic functional connectivity; mild cognitive impairment; multimodal imaging.

Introduction:

In Alzheimer's disease (AD), there is an intricate relationship between amyloid- β ($A\beta$) pathology and the brain's ongoing activity. In particular, the deposition of plaques has been associated with the default mode network (DMN) which is characterized by synchronous infra-slow ongoing activity (i.e. intrinsic functional connectivity [iFC]) [1–6]. This association has been derived due to the striking spatial overlap between $A\beta$ plaque accumulation and the extent of the DMN. The spatial correspondence, together with consistent DMN alterations in AD for iFC [7–9], metabolism [1,2], and structure [10], have led to the proposal of accumulating $A\beta$ pathology along DMN nodes, i.e. along functionally connected rather than spatially neighboring areas [6,11–17]. However, the observed spatial overlap hints at two types of relationship: on the one hand, $A\beta$ pathology disrupts local iFC [6,18–23] while on the other hand, it exhibits a more “positive” relationship—wherever iFC is high, $A\beta$ tends to be high—suggesting a distribution of $A\beta$ following iFC [6,12,17,18,24] .

Crucially, in a previous work of our group, Myers et al. (2014) offered a novel approach to clarify the intricate relationship between $A\beta$ and iFC using a within-subject spatial correlation approach. Looking at several intrinsic networks in a sample of

individuals with prodromal AD, they revealed two distinct effects of A β on intrinsic connectivity. At the global network level they found a positive correspondence, where A β aggregates in areas of high intrinsic connectivity. While at the local network level, they reported a negative correspondence, where plaques load was negatively associated with connectivity. They found significant results across heteromodal networks, with the strongest effect in the posterior DMN (pDMN). However, this work only examined the prodromal stage of AD, and further clarification is needed about the temporal progression of the within-network effects of A β pathology across the stages of the disease. While this previous work provides both the theoretical and methodological backbone of the current study, we aimed at extending those findings by examining the global and local spatial correspondence between A β load and iFC within the pDMN in individual patients across stages of AD and healthy older adults.

In the present study, we used a cross-sectional design involving multimodal imaging data of a rich data sample, including healthy A β negative individuals, as well as preclinical, prodromal, and clinically manifest stages of AD. Within-subject voxel-wise correlations, were used to derive measures of global and local spatial correspondence between A β load and iFC. Based on previous findings from Myers et al. (2014), we hypothesized a

positive global and a negative local spatial correspondence starting with A β accumulation [24,25]. Both processes were expected to reach a plateau at prodromal stages.

Materials and Methods:

Data used in the preparation of this article were obtained from the Alzheimer's Disease Neuroimaging Initiative (ADNI) database (adni.loni.usc.edu). The ADNI was launched in 2003 as a public-private partnership, led by Principal Investigator Michael W. Weiner, MD. The primary goal of ADNI has been to test whether serial magnetic resonance imaging (MRI), positron emission tomography (PET), other biological markers, and clinical and neuropsychological assessment can be combined to measure the progression of mild cognitive impairment (MCI) and early Alzheimer's disease (AD).

Study participants gave written informed consent. The study was approved by local ethic committees in awareness of the Code of Ethics of the World Medical Association (Declaration of Helsinki). A fuller description of ADNI and up-to-date information is available at www.adni-info.org (www.loni.usc.edu/ADNI/) [26–28].

Participants and imaging data:

Within the ADNI-GO and ADNI2 database, all available subjects with resting-state fMRI, AV-45-PET (Florbetapir) and structural MRI were identified (n=149). The maximal time-lag between scans allowed was three months. We identified subjects with resting-state fMRI, AV-45-PET (Florbetapir) and structural MRI from the ADNI-GO and ADNI2 extensions (n=149). Multi-modal data were acquired on multiple scanners using scanners-specific acquisition protocols (see Supplement). Participants included in the analysis were visually inspected and A β positive with exception of CN-. A β negative cognitively impaired participants were excluded from further analysis. A β positivity was defined using a cutoff of 1.11 composite cortical standard uptake value ratio (SUVR) using the cerebellum as a reference [29]. The final sample consisted of 90 participants: 20 CN-, 9 CN+, 21 patients with eMCI+, 18 patients with IMCI+ and 22 patients with AD+ (demographics on Table 1). More details are found in the Supplement and on the ADNI website (<http://adni.loni.usc.edu/methods/>).

MRI Data preprocessing:

Statistical Parametric Mapping Version 8 (SPM8, <http://www.fil.ion.ucl.ac.uk/spm/>) and Data Processing Assistant for Resting State fMRI (DPARSF, <http://rfmri.org/DPARSF>) [30] were used for data preprocessing. After discarding the first three functional images of every subject, we used rigid coregistration to

motion-correct the resting-state fMRI data. We observed no excessive head motion (i.e. cumulative translation or rotation 3mm or 3° and mean point-to-point translation or rotation 0.15 mm or 0.1°). Framewise displacement [31] was not different across groups ($P>0.05$, ANOVA and post-hoc t-tests). The structural image was then coregistered to the mean functional MRI image (using rigid registration), segmented into gray matter, white matter and cerebrospinal fluid, and registered to the Montreal Neurological Institute (MNI) stereotactic space template using unified segmentation. After nuisance regression of head motion, white matter, cerebrospinal fluid, and global signal [30], the same normalization parameters were then used to normalize the functional images into MNI space with an isotropic voxel size of $3 \times 3 \times 3 \text{ mm}^3$. Normalized functional images were finally smoothed with an $8 \times 8 \times 8 \text{ mm}^3$ Gaussian kernel.

As our analysis focused on the correspondence between A β load and iFC, we had to account for nonspecific white matter binding of AV-45 (our proxy for A β load), which has been reported in healthy subjects and patients with AD [32]. Therefore, we created a gray matter mask to ensure that following analyses were restricted to gray matter. More specifically, gray matter segmented images derived from anatomical data were used to create a subject-specific

binarized gray matter mask with a probability threshold of 0.5.

Individual masks were included in all further analyses.

Resting-state fMRI data preprocessing:

Based on previous findings showing the pDMN to be the primary network affected by both A β deposition and iFC reduction

[5,9,24], we explicitly focused our analyses on the pDMN.

Preprocessed data were decomposed into 35 spatially independent components reflecting intrinsic brain networks via a group-level independent component analysis (ICA) framework [33], using the Group ICA of fMRI Toolbox (GIFT,

<http://www.icatb.sourceforge.net>). To automatically select the

pDMN, we applied multiple spatial regression analyses on the 35 independent components using publicly available network

templates from a multicenter study [34]. Then, for each subject an

individual independent component reflecting the pDMN was

derived via back-reconstruction as implemented in GIFT. The

component was composed of the network's time course and spatial

map of z-scores. Voxels with high iFC within the network have

high z-scores, whereas voxels that are not part of the network have

z-scores near 0. Individual levels of pDMN iFC were derived from

voxels with z-values ≥ 1 and with a gray matter probability ≥ 0.5 .

A z-threshold of 1 was set in order to omit negative z-values

reflecting voxels negatively correlated to pDMN activity but to

ensure that the whole extent of the pDMN was included in the analyses (see Figure S1 A, showing a one-sample t-test over all subject, of the thresholded pDMN used in further analyses). Group comparisons of averaged pDMN iFC z-values were performed within one ANOVA model (specified later on) and related post-hoc t-tests ($p < 0.05$, Figure S1).

PET data preprocessing:

Subjects' AV-45-PET scans were rigidly coregistered to their corresponding structural MRI image and then normalized on the MNI template using the previously acquired normalization parameters. This procedure resulted in structural MRI, resting-state fMRI and PET data with identical dimensions and in the same space. For each subject, all voxel values were converted to SUVRs by scaling to the cerebellum as reference. Additionally, images were smoothed using an $8 \times 8 \times 8 \text{ mm}^3$ Gaussian kernel. In order to derive individual measures of A β load, individual AV-45-SUVRs were averaged across those voxels belonging to the individual pDMN mask (i.e., voxels with z-value ≥ 1 , and gray matter probability ≥ 0.5). The individual pDMN masks were derived by back-reconstructing the pDMN derived from the group-level independent component analysis on resting-state fMRI data, as described in the previous section. In order to assess group differences in A β load, individual averaged pDMN AV-45 SUVRs

were entered into the aforementioned ANOVA model and post-hoc t-tests were performed ($p < 0.05$, Figure S1).

Multimodal Analysis:

To study the correspondence between A β load and iFC, we followed the multimodal analysis approach of Myers et al. (2014). The in-home used Matlab scripts are publicly available online, together with a manual and a user-friendly graphical user interface (<https://github.com/TUMnicMuenchen/LocosR>). Briefly, for all network-identified voxels we extracted AV-45 uptake and connectivity values. The global spatial correspondence between A β load and iFC was assessed for each subject using spatial correlation coefficients (Spearman) between voxel-wise AV-45 SUVR and iFC z-values across pDMN voxels, $r_{\text{GLOBAL}}(\text{A}\beta, \text{iFC})$. Resulting $r_{\text{GLOBAL}}(\text{A}\beta, \text{iFC})$ values were Fisher-z-transformed [35], and submitted to the aforementioned ANOVA model. Spearman correlation coefficients were calculated, given that a skewed distribution of connectivity values was induced by applying a z-threshold of 1. In order to investigate the association of A β load and iFC levels within the pDMN with global correspondence, we correlated averaged iFC z-values and averaged AV-45 uptake within the pDMN with $r_{\text{GLOBAL}}(\text{A}\beta, \text{iFC})$ in A β positive subjects (Pearson's correlation coefficient, $p < 0.05$).

To investigate the local impact of A β load on iFC, we derived local spatial correlations between AV-45-SUVr and z-values of pDMN iFC - $r_{\text{LOCAL}}(\text{A}\beta, \text{iFC})$ - via a searchlight approach previously used by our group [6] (see also Supplementary Methods). In order to account for the aforementioned global correspondence, we first orthogonalized AV-45-SUVr and iFC z-values across the whole network at a voxel-wise level, ensuring a global correlation of 0. Then, within a sphere (6 mm radius), the Spearman correlation coefficient between AV-45-SUVr and iFC z-values was calculated for that specific group of voxels, Fisher-z-transformed [35], and assigned to the central voxel of the sphere. This procedure was repeated for each voxel in the brain resulting in individual spatial maps of $r_{\text{LOCAL}}(\text{A}\beta, \text{iFC})$ values within the pDMN of each subject. For each diagnostic group, we submitted the maps to one-sample t-tests and performed voxel-wise group comparisons via an ANOVA model using SPM8. Finally, in order to investigate the association between local correspondence with both local iFC and A β levels within connectivity centers of the pDMN, we extracted the first eigenvariate for AV-45 uptake, iFC z-values and $r_{\text{LOCAL}}(\text{A}\beta, \text{iFC})$ from the main effect of group cluster derived from the aforementioned ANOVA. Averaged levels of AV-45 uptake and iFC z-values were related to $r_{\text{LOCAL}}(\text{A}\beta, \text{iFC})$ via Pearson's correlation analyses ($p < 0.05$). Averaged levels of

$r_{\text{LOCAL}}(\text{A}\beta, \text{iFC})$ derived from the main effect of group cluster were also entered into the aforementioned ANOVA model. One single ANOVA model was used, that included mean iFC z-values within the pDMN, mean AV-45 SUVR within the pDMN, the multimodal measure for global correspondence, and averaged levels of local correspondence derived from the main effect of group cluster. In order to partially correct for atrophy and for our thresholding approach involving both grey matter and iFC z-values, the individual number of voxels included in the analyses were added to the ANOVA model. Additional control analyses for grey matter were performed and are presented in the Supplement.

Results:

Positive spatial correlation between patterns of AV-45 uptake and iFC z-scores across stages of AD and healthy older adults - $r_{\text{GLOBAL}}(\text{A}\beta, \text{iFC})$:

We examined the global correspondence between A β load and iFC in the pDMN across groups via $r_{\text{GLOBAL}}(\text{A}\beta, \text{iFC})$. We found a main effect of group on the global spatial correlation between AV-45 uptake and iFC z-values within the pDMN (Figure 1A, $F=4.60$, $p<0.05$). More specifically, $r_{\text{GLOBAL}}(\text{A}\beta, \text{iFC})$ was positive in A β positive subjects and reached a plateau already in eMCI+, i.e. comparable levels of $r_{\text{GLOBAL}}(\text{A}\beta, \text{iFC})$ were found between eMCI+, lMCI+, and AD+. Findings for $r_{\text{GLOBAL}}(\text{A}\beta, \text{iFC})$ were

robust against atrophy patterns in the whole pDMN (supplementary Figure S2A and B). In the A β positive groups, we further found a positive correlation between $r_{\text{GLOBAL}}(\text{A}\beta, \text{iFC})$ and mean iFC z-values (Figure 1B, $R=0.57$ $p<0.05$). Further, we found a positive correlation between $r_{\text{GLOBAL}}(\text{A}\beta, \text{iFC})$ and mean AV-45 uptake within the pDMN (Figure 1C, $R=0.28$ $p<0.05$).

Negative local correlation between AV-45 uptake and iFC z-scores across stages of AD and healthy older adults -

$r_{\text{LOCAL}}(\text{A}\beta, \text{iFC})$:

Next we examined the local “negative” impact of A β load on iFC within the pDMN across the AD stages and healthy older adults. Specifically, after taking into consideration the variability in A β pathology that is determinable through $r_{\text{GLOBAL}}(\text{A}\beta, \text{iFC})$, we expected that a neurotoxic effect of higher load should lead to a “relative decrease” in intrinsic connectivity, in cores with high connectivity. In order to account for the global correspondence, we first orthogonalized A β and iFC at the global level. Then we used a searchlight approach to calculate the local spatial correlation of AV-45 uptake and iFC z-values i.e., $r_{\text{LOCAL}}(\text{A}\beta, \text{iFC})$. Figure 2A, shows voxel-wise $r_{\text{LOCAL}}(\text{A}\beta, \text{iFC})$ maps reflecting the local detrimental effect of A β load on iFC within the pDMN across all groups (Figure 2A panel a, one-sample t-test $p<0.05$ FWE corrected) and the main effect of group (Figure 2A

panel b, ANOVA $p < 0.05$ FWE corrected). Post-hoc group comparisons revealed significantly enhanced detrimental effects of local A β load on iFC in the patient groups, particularly in the precuneus and posterior cingulate of patients with eMCI+, IMCI+ and AD+ when compared to CN- (Figure 2A panels c-e, post-hoc t-tests $p < 0.05$ FWE corrected). This voxel-wise analysis revealed no significant differences among the patient groups or when comparing any group to CN+.

To further analyze $r_{\text{LOCAL}}(\text{A}\beta, \text{iFC})$ across stages of AD in relation to both iFC and A β , we extracted and plotted the first eigenvariate values for $r_{\text{LOCAL}}(\text{A}\beta, \text{iFC})$ from the group effect cluster of the voxel-wise ANOVA. The ANOVA of averaged $r_{\text{LOCAL}}(\text{A}\beta, \text{iFC})$ scores produced analogous results to the voxel-wise analysis (Figure 2B, $F = 8.34$, $p < 0.05$). Findings for $r_{\text{LOCAL}}(\text{A}\beta, \text{iFC})$ were robust against atrophy patterns within the $r_{\text{LOCAL}}(\text{A}\beta, \text{iFC})$ cluster (supplementary Figure S2C and D). We then analyzed the relation between detrimental A β effects on iFC, and available levels of A β and iFC in A β positive subjects. We correlated mean levels of iFC and A β load, respectively, with $r_{\text{LOCAL}}(\text{A}\beta, \text{iFC})$, extracted from the group effect cluster from the previous voxel-wise analysis. We found a negative correlation between $r_{\text{LOCAL}}(\text{A}\beta, \text{iFC})$ and averaged iFC z-values (Figure 2C, $R = -0.43$ $p < 0.05$). In contrast,

no significant correlation was found between $r_{\text{LOCAL}}(\text{A}\beta, \text{iFC})$ and AV-45 uptake (Figure 2D, $R=0.03$ $p=0.82$).

Discussion:

Across the AD spectrum, we report a positive within-subject global correspondence between A β distribution and iFC of the pDMN (Figure 1). This outcome was anticipated and is in line with the well-known spatial overlap between the pDMN and A β deposition [1]. Critically, such global correspondence starts in preclinical stages CN+ and reached a definitive plateau in early symptomatic stages of MCI (i.e., eMCI+), demonstrating a non-linear trajectory of correlated iFC and A β distribution. To clarify, a within-subject positive correlation between voxel-wise iFC and voxel-wise AV45-uptake, i.e. $r_{\text{GLOBAL}}(\text{A}\beta, \text{iFC})$, indicates that voxels in the network core (i.e. voxels with high iFC) were burdened with higher A β deposition than the network periphery (voxels with low iFC). No significant differences were observed in the global correspondence of A β load and iFC between the different stages of the disease (eMCI+, IMCI+, AD+). This data suggests that the deposition of A β in areas of high iFC within the pDMN already starts in the earliest clinical stages of AD while reaching a plateau as the disease progresses. This finding is consistent with previous studies showing extensive A β deposition within regions of the pDMN at early disease stages, which slows down as the disease advances and saturated levels of A β are reached [36–38]. Critically, increased $r_{\text{GLOBAL}}(\text{A}\beta, \text{iFC})$ within the pDMN correlated

positively with levels of global iFC and levels of global A β within the whole pDMN in A β positive subjects. This result suggest a mechanistic process, in which available levels of iFC within the pDMN may determine A β deposition in areas of high iFC, and finally global levels of A β load.

We examined additionally the within-subject local correspondence between A β load and iFC of the pDMN across groups (Figure 2), after orthogonalization of A β load and iFC at the global level, in order to account for the global correspondence as implemented in Myers et al. (2014). We found a significant negative local correlation between A β load and iFC particularly in patients' precuneus and posterior cingulate, which are primarily affected by A β load [2,3,5,6,24]. To further elucidate, a locally delimited negative correlation between voxel-wise iFC and voxel-wise AV45-uptake within connectivity centers of the pDMN, i.e. $r_{\text{LOCAL}}(\text{A}\beta, \text{iFC})$, suggests that A β pathology adversely affects intrinsic connectivity within connectivity centers of the pDMN as a function of local A β -plaque concentration. Critically, the local negative correspondence between A β load and iFC was enhanced along the AD spectrum, starting already at preclinical stages (CN+) and reaching a peak in eMCI+. This finding suggests that the negative effects of A β load on iFC are located particularly within centers of the pDMN, start in preclinical stages of CN+, and peak

with appearance of first cognitive symptoms. Extending the work of Myers and colleagues using the same methods, but restricted to a sample with early MCI [6], we found a negative association between mean $r_{\text{LOCAL}}(\text{A}\beta, \text{iFC})$ and mean levels of iFC within connectivity centers of the pDMN across subjects of the AD spectrum. These findings indicate that negative $\text{A}\beta$ effects on iFC are the stronger, the higher individual levels of iFC. In contrast, no significant correlation was found between mean $r_{\text{LOCAL}}(\text{A}\beta, \text{iFC})$ and mean levels of network $\text{A}\beta$ load, suggesting threshold effects. These findings suggest that detrimental effects of $\text{A}\beta$ load on iFC are stable from eMCI+ on, and determined rather by the strength of individual iFC levels than from $\text{A}\beta$ levels.

Our results provide insights about the inter-relatedness of $\text{A}\beta$, iFC, and their global and local correspondence within the pDMN across stages of AD. We have summarized our findings as a trajectory model for the pDMN in Figure 3, proposing a temporal order of changes in $\text{A}\beta$ and $r_{\text{GLOBAL}}(\text{A}\beta, \text{iFC})$, as well as iFC and $r_{\text{LOCAL}}(\text{A}\beta, \text{iFC})$ across the AD spectrum. In particular, we propose an interaction model of distinct global and local processes between $\text{A}\beta$ and iFC, which start at the preclinical stage. In the preclinical stage, where the first signs of $\text{A}\beta$ pathology are detectable in the absence of symptoms, $\text{A}\beta$ accumulation increases, reaching a plateau in early clinical disease stages. In parallel to the

rise of $A\beta$ accumulation, the global correspondence between $A\beta$ and iFC, $r_{\text{GLOBAL}}(A\beta, \text{iFC})$, begins also to rise, suggesting that iFC of the pDMN determines the accumulation levels of $A\beta$ within the network, reaching a plateau in early disease stages.

Network-framed $A\beta$ accumulation is accompanied by local negative effects of $A\beta$ pathology on iFC in network centers, where both iFC and $A\beta$ accumulation have their peaks [39]. Such detrimental local processes take place already in preclinical stages and reach a peak in eMCI+ with the appearance of first cognitive symptoms. The detrimental effect of $A\beta$ on iFC is accompanied by progressive iFC reduction of the pDMN [7–9]. The detrimental $A\beta$ effect is constant when certain levels of $A\beta$ are reached, but it is stronger when individual iFC levels are higher (Figure 2C). With further iFC reductions along disease progression, the detrimental effect of $A\beta$ on iFC is slightly weakened. Because of progressive iFC decreases across the disease trajectory, we suggest that other factors such as “nodal stress”, in which hub regions undergo activity-related degradation, neuroinflammatory and vascular processes, or increasing tau-based neurodegeneration might become more relevant for iFC decreases, and as a consequence network dysfunction, than constant $A\beta$ effects [4,40,41].

In summary, our model is in line with previous hypotheses stating that propagating $A\beta$ accumulation follows a network-based pattern

[6,11,12,15,17]. However, it proposes that when accounting for the global effect of iFC on A β pathology accumulation, simultaneous local detrimental effects of A β load on iFC start in centers of higher iFC and pathology levels. In other words, wherever A β accumulation exceeds a specific threshold, accumulated pathology exerts a stable long-lasting negative influence on local iFC. In our model, both A β pathology accumulation and its detrimental effects on iFC start already at presymptomatic stages of AD, reaching a peak and stabilizing with the emergence of first cognitive symptoms at eMCI+. This starting point highlights the need for an effective characterization and further stratification of preclinical stages, where therapeutic interventions could have the most promising effect.

Several limitations need to be considered. First, though our model implicates trajectory of changes, our data is cross-sectional.

Longitudinal studies are necessary to test the course of correspondence between A β load and iFC, with a special focus on non-linear relationships between iFC and A β along disease progression, which we did not account for in the current study.

Second, based on previous work of our group finding the strongest effect in the pDMN, our study strictly focuses on this network, neglecting that other DMN subsystems [4] and heteromodal networks [5] are affected by A β pathology and iFC changes across

stages of AD. A previous study from our group reported similar effects of global and local correspondence between A β and iFC in heteromodal networks of patients with MCI, though the effects were of lesser magnitude [6]. We hypothesize that similar trajectories may take place in distinct heteromodal networks but with a delayed onset in respect to the pDMN, following a cross-network gradient [6]. However, recent literature has revealed patterns of non-linearly progressing changes of iFC in AD, most notably within some subsystems of the DMN [5]. Moreover, increases in iFC have been reported both at the intrinsic brain network level – e.g. within the Salience Network [42] – and at the regional level – e.g. increased iFC locally confined within the MTL [43], [44]. In order to assess general conclusions on the relationship between A β and iFC across stages of AD, our findings need to be extended to other intrinsic brain networks, and need to be completed by the use of complementary iFC measures, such as inter-network functional connectivity and degree centrality. Finally, our study is focused on the correspondence between A β pathology and iFC, ignoring that tau-based pathology and neurodegeneration might critically modulate such correspondence [4,41]. Future studies might include measures reflecting tau-based neurodegeneration in order to draw a more detailed picture.

Financial disclosures:

All authors declare that the research was conducted in the absence of any commercial or financial relationships that could be construed as a potential conflict of interest.

Funding:

This work was supported by the Deutsche Forschungsgemeinschaft (grant 621553 to C.S.), the Alzheimer Forschungs Initiative (grant 12819 to C.S.), the German Academic Foundation (to L.P.) and the Kommission für Klinische Forschung of the Klinikum rechts der Isar der Technischen Universität München (grant 8765162 to C.S).

Data collection and sharing for this project was funded by the Alzheimer's Disease Neuroimaging Initiative (ADNI) (National Institutes of Health Grant U01 AG024904) and DOD ADNI (Department of Defense award number W81XWH-12-2-0012).

ADNI is funded by the National Institute on Aging, the National Institute of Biomedical Imaging and Bioengineering, and through generous contributions from the following: AbbVie, Alzheimer's Association; Alzheimer's Drug Discovery Foundation; Araclon Biotech; BioClinica, Inc.; Biogen; Bristol-Myers Squibb Company; CereSpir, Inc.; Cogstate; Eisai Inc.; Elan Pharmaceuticals, Inc.; Eli Lilly and Company; EuroImmun; F. Hoffmann-La Roche Ltd and its affiliated company Genentech,

nc.; Fujirebio; GE Healthcare; IXICO Ltd.; Janssen Alzheimer Immunotherapy Research & Development, LLC.; Johnson & Johnson Pharmaceutical Research & Development LLC.; Lumosity; Lundbeck; Merck & Co., Inc.; Meso Scale Diagnostics, LLC.; NeuroRx Research; Neurotrack Technologies; Novartis Pharmaceuticals Corporation; Pfizer Inc.; Piramal Imaging; Servier; Takeda Pharmaceutical Company; and Transition Therapeutics. The Canadian Institutes of Health Research is providing funds to support ADNI clinical sites in Canada. Private sector contributions are facilitated by the Foundation for the National Institutes of Health (www.fnih.org). The grantee organization is the Northern California Institute for Research and Education, and the study is coordinated by the Alzheimer's Therapeutic Research Institute at the University of Southern California. ADNI data are disseminated by the Laboratory for Neuro Imaging at the University of Southern California.

References:

- [1] Buckner RL, Snyder AZ, Shannon BJ, LaRossa G, Sachs R, Fotenos AF, Sheline YI, Klunk WE, Mathis CA, Morris JC, Mintun MA (2005) Molecular, structural, and functional characterization of Alzheimer's disease: evidence for a relationship between default activity, amyloid, and memory. *J Neurosci* **25**, 7709–7717.
- [2] Drzezga A, Becker JA, Van Dijk KR a, Sreenivasan A, Talukdar T, Sullivan C, Schultz AP, Sepulcre J, Putcha D, Greve D, Johnson K a., Sperling R a. (2011) Neuronal dysfunction and disconnection of cortical hubs in non-demented subjects with elevated amyloid burden. *Brain* **134**, 1635–1646.
- [3] Elman JA, Madison CM, Baker SL, Vogel JW, Marks SM, Crowley S, O'Neil JP, Jagust WJ (2016) Effects of Beta-Amyloid on Resting State Functional Connectivity Within and Between Networks Reflect Known Patterns of Regional Vulnerability. *Cereb Cortex* **26**, 695–707.
- [4] Sperling R, Mormino E, Johnson K (2014) The evolution of preclinical Alzheimer's disease: implications for prevention trials. *Neuron* **84**, 608–622.
- [5] Jones DT, Knopman DS, Gunter JL, Graff-Radford J, Vemuri P, Boeve BF, Petersen RC, Weiner MW, Jack CR

- (2016) Cascading network failure across the Alzheimer's disease spectrum. *Brain* **139**, 547–562.
- [6] Myers N, Pasquini L, Göttler J, Grimmer T, Koch K, Ortner M, Neitzel J, Mühlau M, Förster S, Kurz A, Förstl H, Zimmer C, Wohlschläger AM, Riedl V, Drzezga A, Sorg C (2014) Within-patient correspondence of amyloid- β and intrinsic network connectivity in Alzheimer's disease. *Brain* **137**, 2052–2064.
- [7] Greicius MD, Srivastava G, Reiss AL, Menon V (2004) Default-mode network activity distinguishes Alzheimer's disease from healthy aging: evidence from functional MRI. *Proc Natl Acad Sci U S A* **101**, 4637–4642.
- [8] Lim HK, Nebes R, Snitz B, Cohen A, Mathis C, Price J, Weissfeld L, Klunk W, Aizenstein HJ (2014) Regional amyloid burden and intrinsic connectivity networks in cognitively normal elderly subjects. *Brain* **137**, 3327–3328.
- [9] Sorg C, Riedl V, Mühlau M, Calhoun VD, Eichele T, Lär L, Drzezga A, Förstl H, Kurz A, Zimmer C, Wohlschläger AM (2007) Selective changes of resting-state networks in individuals at risk for Alzheimer's disease. *Proc Natl Acad Sci U S A* **104**, 18760–18765.
- [10] Ossenkoppele R, Cohn-Sheehy BI, La Joie R, Vogel JW, Möller C, Lehmann M, van Berckel BNM, Seeley WW,

- Pijnenburg YA, Gorno-Tempini ML, Kramer JH, Barkhof F, Rosen HJ, van der Flier WM, Jagust WJ, Miller BL, Scheltens P, Rabinovici GD (2015) Atrophy patterns in early clinical stages across distinct phenotypes of Alzheimer's disease. *Hum Brain Mapp* **36**, 4421–4437.
- [11] Frost B, Diamond MI (2010) Prion-like mechanisms in neurodegenerative diseases. *Nat Rev Neurosci*. **11**, 155–159.
- [12] Iturria-Medina Y, Sotero RC, Toussaint PJ, Evans AC (2014) Epidemic spreading model to characterize misfolded proteins propagation in aging and associated neurodegenerative disorders. *PLoS Comput Biol* **10**, e1003956.
- [13] Klupp E, Förster S, Grimmer T, Tahmasian M, Yakushev I, Sorg C, Yousefi BH, Drzezga A (2014) In Alzheimer's disease, hypometabolism in low-amyloid brain regions may be a functional consequence of pathologies in connected brain regions. *Brain Connect* **4**, 371–383.
- [14] Klupp E, Grimmer T, Tahmasian M, Sorg C, Yakushev I, Yousefi BH, Drzezga A, Förster S (2015) Prefrontal hypometabolism in Alzheimer disease is related to longitudinal amyloid accumulation in remote brain regions. *J Nucl Med* **56**, 399–404.
- [15] Nath S, Agholme L, Kurudenkandy FR, Granseth B,

- Marcusson J, Hallbeck M (2012) Spreading of neurodegenerative pathology via neuron-to-neuron transmission of β -amyloid. *J Neurosci* **32**, 8767–8777.
- [16] Seeley WW, Crawford RK, Zhou J, Miller BL, Greicius MD (2009) Neurodegenerative Diseases Target Large-Scale Human Brain Networks. *Neuron* **62**, 42–52.
- [17] Zhou J, Gennatas ED, Kramer JH, Miller BL, Seeley WW (2012) Predicting regional neurodegeneration from the healthy brain functional connectome. *Neuron* **73**, 1216–1227.
- [18] Bero AW, Yan P, Roh JH, Cirrito JR, Stewart FR, Raichle ME, Lee J-M, Holtzman DM (2011) Neuronal activity regulates the regional vulnerability to amyloid- β deposition. *Nat Neurosci* **14**, 750–756.
- [19] Busche MA, Eichhoff G, Adelsberger H, Abramowski D, Wiederhold K-H, Haass C, Staufenbiel M, Konnerth A, Garaschuk O (2008) Clusters of hyperactive neurons near amyloid plaques in a mouse model of Alzheimer's disease. *Science* **321**, 1686–1689.
- [20] Busche MA, Chen X, Henning HA, Reichwald J, Staufenbiel M, Sakmann B, Konnerth A (2012) Critical role of soluble amyloid- β for early hippocampal hyperactivity in a mouse model of Alzheimer's disease. *Proc Natl Acad Sci*

U S A **109**, 8740–8745.

- [21] Busche MA, Kekuš M, Adelsberger H, Noda T, Förstl H, Nelken I, Konnerth A (2015) Rescue of long-range circuit dysfunction in Alzheimer’s disease models. *Nat Neurosci* **18**, 1623–1630.
- [22] Mormino EC, Brandel MG, Madison CM, Marks S, Baker SL, Jagust WJ (2012) A β Deposition in aging is associated with increases in brain activation during successful memory encoding. *Cereb Cortex* **22**, 1813–1823.
- [23] Sheline YI, Raichle ME (2013) Resting state functional connectivity in preclinical Alzheimer’s disease. *Biol Psychiatry* **74**, 340–347.
- [24] Grothe MJ, Teipel SJ (2016) Spatial patterns of atrophy, hypometabolism, and amyloid deposition in Alzheimer’s disease correspond to dissociable functional brain networks. *Hum Brain Mapp* **37**, 35–53.
- [25] Engler H, Forsberg A, Almkvist O, Blomquist G, Larsson E, Savitcheva I, Wall A, Ringheim A, Långström B, Nordberg A (2006) Two-year follow-up of amyloid deposition in patients with Alzheimer’s disease. *Brain* **129**, 2856–2866.
- [26] Jagust WJ, Bandy D, Chen K, Foster NL, Landau SM, Mathis CA, Price JC, Reiman EM, Skovronsky D, Koeppe RA (2010) The Alzheimer’s Disease Neuroimaging

- Initiative positron emission tomography core. *Alzheimer's Dement* **6**, 221–229.
- [27] Langbaum JBS, Chen K, Lee W, Reschke C, Bandy D, Fleisher AS, Alexander GE, Foster NL, Weiner MW, Koeppe RA, Jagust WJ, Reiman EM (2009) Categorical and correlational analyses of baseline fluorodeoxyglucose positron emission tomography images from the Alzheimer's Disease Neuroimaging Initiative (ADNI). *Neuroimage* **45**, 1107–1116.
- [28] Mueller SG, Weiner MW, Thal LJ, Petersen RC, Jack CR, Jagust W, Trojanowski JQ, Toga AW, Beckett L (2005) Ways toward an early diagnosis in Alzheimer's disease: the Alzheimer's Disease Neuroimaging Initiative (ADNI). *Alzheimer's Dement* **1**, 55–66.
- [29] Fleisher a. S, Chen K, Liu X, Roontiva a., Thiyyagura P, Ayutyanont N, Joshi a. D, Clark CM, Mintun M a., Pontecorvo MJ, Doraiswamy PM, Johnson K a., Skovronsky DM, Reiman EM (2011) Using Positron Emission Tomography and Florbetapir F 18 to Image Cortical Amyloid in Patients With Mild Cognitive Impairment or Dementia Due to Alzheimer Disease. *Arch Neurol* **68**, 1404–1411.
- [30] Chao-Gan Y, Yu-Feng Z (2010) DPARSF: A MATLAB

Toolbox for “Pipeline” Data Analysis of Resting-State
fMRI. *Front Syst Neurosci* **4**, 13.

- [31] Power JD, Barnes K a., Snyder AZ, Schlaggar BL, Petersen SE (2012) Spurious but systematic correlations in functional connectivity MRI networks arise from subject motion. *Neuroimage* **59**, 2142–2154.
- [32] Edison P, Carter SF, Rinne JO, Gelosa G, Herholz K, Nordberg A, Brooks DJ, Hinz R (2013) Comparison of MRI based and PET template based approaches in the quantitative analysis of amyloid imaging with PIB-PET. *Neuroimage* **70**, 423–433.
- [33] Calhoun VD, Adali T, Pearlson GD, Pekar JJ (2001) Spatial and temporal independent component analysis of functional MRI data containing a pair of task-related waveforms. *Hum Brain Mapp.* **13**, 43–53.
- [34] Allen E a, Erhardt EB, Damaraju E, Gruner W, Segall JM, Silva RF, Havlicek M, Rachakonda S, Fries J, Kalyanam R, Michael AM, Caprihan A, Turner J a, Eichele T, Adelsheim S, Bryan AD, Bustillo J, Clark VP, Feldstein Ewing SW, Filbey F, Ford CC, Hutchison K, Jung RE, Kiehl K a, Kodituwakku P, Komesu YM, Mayer AR, Pearlson GD, Phillips JP, Sadek JR, Stevens M, Teuscher U, Thoma RJ, Calhoun VD (2011) A baseline for the multivariate

- comparison of resting-state networks. *Front Syst Neurosci* **5**, 2.
- [35] Myers L, Sirois MJ (2004) Spearman Correlation Coefficients, Differences between. In *Encyclopedia of Statistical Sciences* John Wiley & Sons, Inc.
- [36] Kadir A, Almkvist O, Forsberg A, Wall A, Engler H, Långström B, Nordberg A (2012) Dynamic changes in PET amyloid and FDG imaging at different stages of Alzheimer's disease. *Neurobiol Aging* **33**,.
- [37] Jack CR, Lowe VJ, Weigand SD, Wiste HJ, Senjem ML, Knopman DS, Shiung MM, Gunter JL, Boeve BF, Kemp BJ, Weiner M, Petersen RC (2009) Serial PIB and MRI in normal, mild cognitive impairment and Alzheimers disease: Implications for sequence of pathological events in Alzheimers disease. *Brain* **132**, 1355–1365.
- [38] Villain N, Chetelat G, Grassiot B, Bourgeat P, Jones G, Ellis KA, Ames D, Martins RN, Eustache F, Salvado O, Masters CL, Rowe CC, Villemagne VL (2012) Regional dynamics of amyloid- deposition in healthy elderly, mild cognitive impairment and Alzheimer's disease: a voxelwise PiB-PET longitudinal study. *Brain* **135**, 2126–2139.
- [39] Buckner RL, Andrews-Hanna JR, Schacter DL (2008) The brain's default network: Anatomy, function, and relevance

- to disease. *Ann N Y Acad Sci.* **1124**, 1–38.
- [40] Chételat G (2013) Reply: The amyloid cascade is not the only pathway to AD. *Nat Rev Neurol* **9**, 356.
- [41] Sorg C, Grothe MJ (2015) The complex link between amyloid and neuronal dysfunction in Alzheimer’s disease. *Brain* **138**, 3472–3475.
- [42] Zhou J, Greicius MD, Gennatas ED, Growdon ME, Jang JY, Rabinovici GD, Kramer JH, Weiner M, Miller BL, Seeley WW (2010) Divergent network connectivity changes in behavioural variant frontotemporal dementia and Alzheimer’s disease. *Brain* **133**, 1352–1367.
- [43] Das SR, Pluta J, Mancuso L, Kliot D, Orozco S, Dickerson BC, Yushkevich PA, Wolk DA (2013) Increased functional connectivity within medial temporal lobe in mild cognitive impairment. *Hippocampus* **23**, 1–6.
- [44] Pasquini L, Scherr M, Tahmasian M, Meng C, Myers NE, Ortner M, Mark M, Kurz A, Hans F (2015) Link between hippocampus ’ raised local and eased global intrinsic connectivity in AD. *Alzheimer's and Dement* **11**, 475–484.
- [45] Kriegeskorte N, Goebel R, Bandettini P (2006) Information-based functional brain mapping. *Proc Natl Acad Sci U S A* **103**, 3863–3868.

Tables:

Table 1. Demographic and neuropsychological data.

	AD+	IMCI+	eMCI+	CN+	CN-	<i>F</i>	p-value
Number n	22	18	21	9	20		
Age, years	73.3 (7.9)	73.5 (7.3)	71.2 (5.6)	76.2 (5.6)	74.6 (7.8)	1.00	0.409
Education (years of school)	15.2 (2.4)	16.3 (2.4)	15.4 (2.6)	16.1 (1.3)	16.3 (2.2)	1.00	0.431
% Female	54.5	44.4	42.8	55.5	70.0	-	0.60
ADAS-Cog	35.5 (10.1)	20.5 (7.7)	14.1 (6.1)	9.2 (3.7)	9.5 (4.3)	44.41	<0.001
MMSE	22.7 (2.8)	27.2 (1.9)	27.6 (1.9)	29.0 (1.1)	29.2 (1.9)	34.42	<0.001

AD+, A β positive Alzheimer's disease; ADAS-Cog, Alzheimer's Disease Assessment Scale Cognitive subscale; eMCI+, A β positive early mild cognitive impairment; IMCI+, A β positive late mild cognitive impairment; MMSE, Mini-mental State Examination; CN-, A β negative cognitively normal subjects; CN+, A β positive cognitively normal subjects. Group comparisons: ANOVA for all measures except gender (Kruskal-Wallis-Test).

Figure Legends:

Figure 1. Global correspondence between A β load and iFC for

the pDMN across the AD spectrum. (A) The global

correspondence between A β load and iFC - $r_{\text{GLOBAL}}(\text{A}\beta, \text{iFC})$ – in

the pDMN is positive and increased across the AD spectrum—

showing that A β aggregates in areas of high intrinsic

connectivity—and reaching a plateau in eMCI+, i.e. comparable

levels of $r_{\text{GLOBAL}}(\text{A}\beta, \text{iFC})$ are found across the patient groups

(ANOVA and related post-hoc t-tests, $p < 0.05$). (B) $r_{\text{GLOBAL}}(\text{A}\beta,$

iFC) correlates positively with mean iFC z-values within the

pDMN (Pearson's correlation coefficient, $p < 0.05$). (C)

$r_{\text{GLOBAL}}(\text{A}\beta, \text{iFC})$ correlates positively with mean AV-45 uptake

within the pDMN (Pearson's correlation coefficient, $p < 0.05$). AD

= Alzheimer's disease; AD+ = A β positive AD; a.u. = arbitrary

units; pDMN = posterior default mode network; eMCI+ = A β

positive early mild cognitive impairment; lMCI+ = A β positive late

mild cognitive impairment; CN- = A β negative cognitively normal

subjects; CN+ = A β positive cognitively normal subjects; SUVR =

standardized uptake value ratio.

Figure 2. The negative local correspondence between A β load and iFC within the pDMN is enhanced across the AD

spectrum. Panel A shows voxel-wise analyses comparing the local

correspondence between A β load and pDMN iFC – (A β , iFC) – across groups. After accounting for regional variability in global correspondence via decorrelation, local spatial correspondence between A β and iFC was calculated by spatial correlations within local spheres via a searchlight approach—indicating that A β pathology reduces connectivity in the pDMN as a function of local plaque concentration. (Aa) One-sample t-test ($p < 0.05$ FWE corrected) among all subject showing t-maps of $r_{\text{LOCAL}}(\text{A}\beta, \text{iFC})$ peaking within posterior connectivity centers of the pDMN i.e., the posterior cingulate and precuneus. (Ab) ANOVA analysis ($p < 0.05$ FWE corrected) showing a main effect of group for $r_{\text{LOCAL}}(\text{A}\beta, \text{iFC})$ in the same posterior connectivity centers described before. (Ac-e) Post-hoc t-tests ($p < 0.05$ FWE corrected) reveal enhanced negative levels of $r_{\text{LOCAL}}(\text{A}\beta, \text{iFC})$ in patients compared to CN- within the posterior cingulate and precuneus. No group differences were detected across patient groups or when compared to CN+. (B) Panel B shows results using the first eigenvariate of $r_{\text{LOCAL}}(\text{A}\beta, \text{iFC})$ derived from the group effect cluster. $r_{\text{LOCAL}}(\text{A}\beta, \text{iFC})$ is negative, peaks in eMCI+, with a plateau-like course for clinical stages, i.e. comparable levels of $r_{\text{LOCAL}}(\text{A}\beta, \text{iFC})$ are found across the patient groups (ANOVA and related post-hoc t-tests, $p < 0.05$). (C) Mean $r_{\text{LOCAL}}(\text{A}\beta, \text{iFC})$ and averaged levels of iFC z-values within connectivity centers of the

pDMN show a significant negative correlation (Pearson's correlation coefficient, $p < 0.05$). (D) Mean $r_{\text{LOCAL}}(\text{A}\beta, \text{iFC})$ and averaged levels of AV-45 uptake within connectivity centers of the pDMN show no significant correlation (Pearson's correlation coefficient, $p < 0.05$). AD = Alzheimer's disease; AD+ = A β positive AD; a.u. = arbitrary units; pDMN = posterior default mode network; eMCI+ = A β positive early mild cognitive impairment; lMCI+ = A β positive late mild cognitive impairment; CN- = A β negative cognitively normal subjects; CN+ = A β positive cognitively normal subjects.

Figure 3. Proposed model for the pDMN trajectory of A β , iFC, and both local and global correspondence between A β and iFC along stages of AD. For visualization purposes, one-sample t-test of the thresholded pDMN maps used in the study in bright green. In the transition phase from healthy to preclinical cognitively normal conditions, where first signs of A β pathology are detected (depicted in yellow in the graph and in the gradient bar below the graph), levels of A β load (A β , line in light green) begin to rise while iFC of the pDMN (iFC, line in orange) gradually decreases. In parallel to increased levels of A β load, the global correspondence between A β load and iFC (i.e., $r_{\text{GLOBAL}}(\text{A}\beta, \text{iFC})$ within the pDMN, line in dark green) begins also to rise,

suggesting increased A β accumulation within regions of the network with higher iFC (iFC associated A β accumulation, gradient bar in green). Analogously, the local correspondence between A β load and iFC within the pDMN (i.e., $r_{\text{LOCAL}}(\text{A}\beta, \text{iFC})$, line in dark red) begins to decrease in preclinical stages of AD, indicating detrimental effects of A β pathology on iFC of pDMN connectivity centers (detrimental effects of A β on iFC, gradient bar in red). Global and local correspondence between A β load and iFC reach a plateau in eMCI+, in parallel with appearance of first cognitive symptoms (as dashed blue line in the graph and blue gradient bar). In a nutshell, in the pDMN A β accumulates in areas of higher iFC in individual patients; and simultaneously, when certain A β levels are reached, A β pathology has detrimental effects on local iFC; both mechanisms emerge already in the preclinical stages of AD when first A β accumulation is present, peak and stabilize at early prodromal stages with the appearance of first cognitive symptoms.

A β = Amyloid- β ; AD = Alzheimer's disease; AD+ = A β positive Alzheimer's disease; pDMN = posterior default mode network; eMCI+ = A β positive early mild cognitive impairment; lMCI+ = A β positive late mild cognitive impairment; CN- = A β negative cognitively normal subjects; CN+ = A β positive cognitively normal subjects.

Figures:

Figure 1:

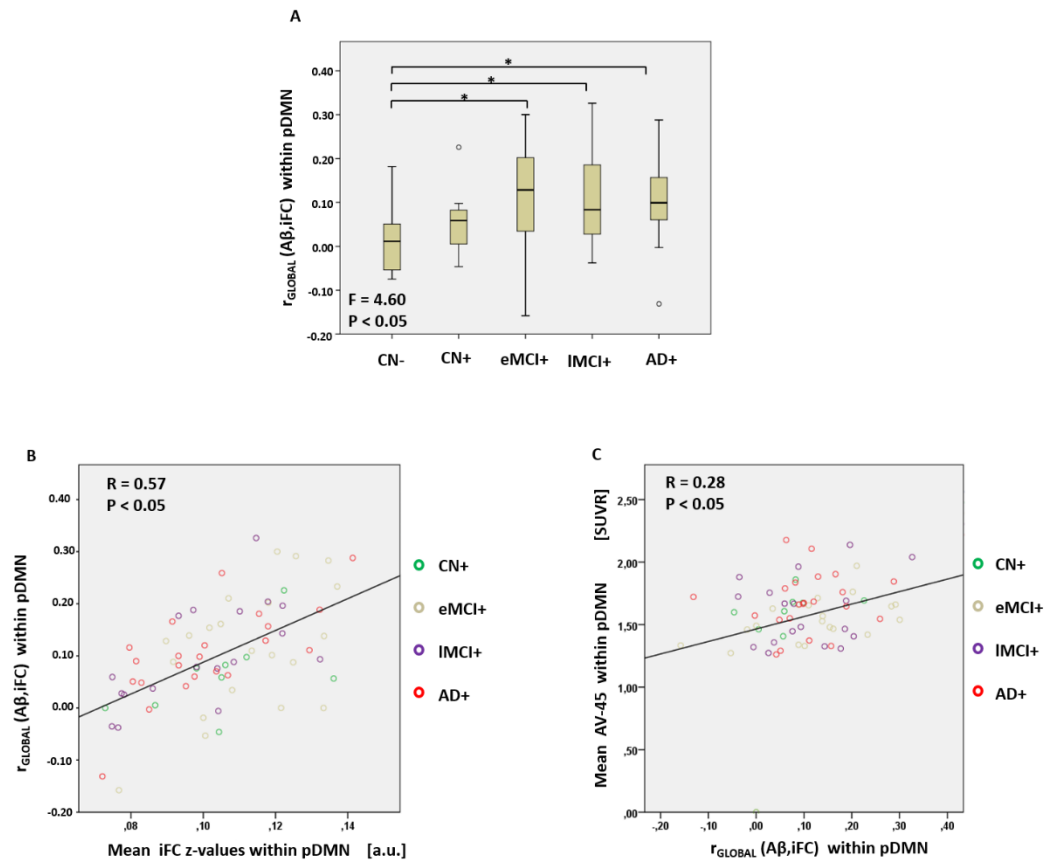


Figure 2:

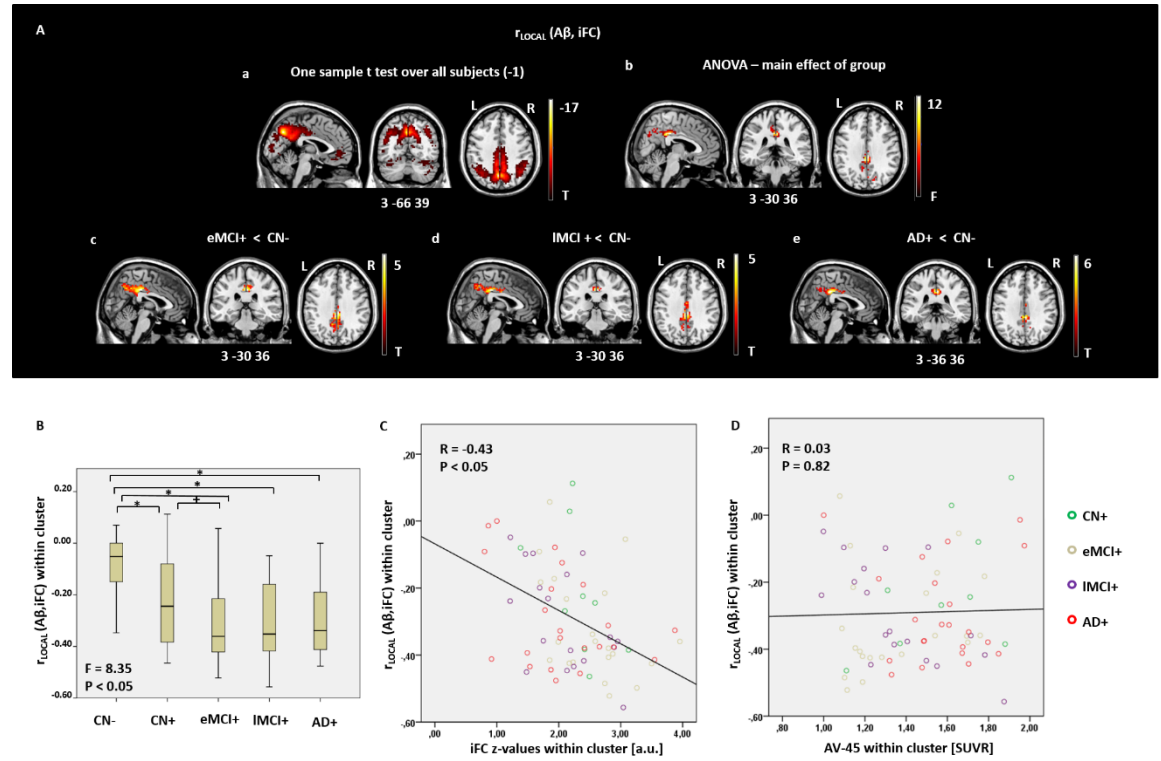
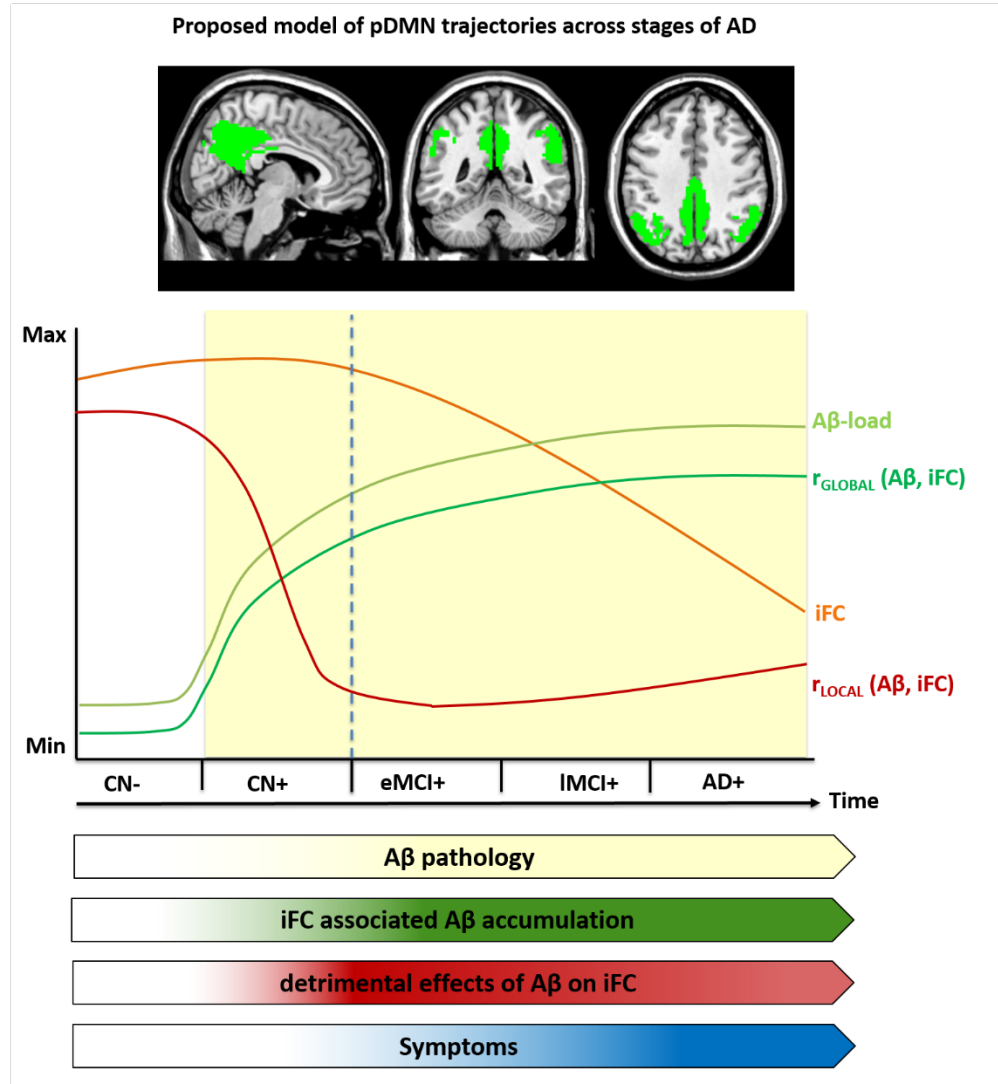


Figure 3:



Supplementary Material for

**Individual correspondence of amyloid- β and intrinsic
connectivity in the posterior default mode network across
stages of Alzheimer's disease**

Lorenzo Pasquini ^{*†1,9}, Gloria Benson ^{†5,9}, Michel J. Grothe ⁶,
Lukas Utz ^{4,9}, Nicholas E. Myers ^{7,9}, Igor Yakushev ^{3,9}, Timo
Grimmer ^{2,9}, Martin Scherr ^{2,8,9}, Christian Sorg ^{2,4,9} for the
Alzheimer's Disease Neuroimaging Initiative⁺.

Supplementary Methods: 4

- Participants:
- Imaging data acquisition:
- Searchlight approach:
- Control for grey matter atrophy:

Supplementary Results: 2

- Increased A β load and decreased iFC within the pDMN
along the AD spectrum:
- Grey matter atrophy is not associated with r_{GLOBAL} (A β ,
iFC) and r_{LOCAL} (A β , iFC):

Supplementary Reference: 3

Supplementary Legends and Figures: 2

- Supplementary Figure S1:
- Supplementary Figure S2:

Supplementary Methods:

Participants:

We identified available subjects with resting-state fMRI, AV-45-PET (florbetapir) and structural MRI from the ADNI-GO and ADNI2 extensions of the ADNI database (n=149). If two resting state functional MRI scans were performed, the scan closest to the AV-45-PET scan date was chosen. All images were visually inspected for quality control and 59 subjects were excluded on several factors: imaging artifacts (n=19), whole brain not covered in field of view (n=7) excessive head motion (n=2) and A β negative participants within the patient group (n=31). All participants included in the analysis (n=90) were A β positive with exception of CN-. Cognitively impaired participants who were A β negative were excluded from further analysis. A β positivity was defined as suggested by ADNI methods of florbetapir analysis using a cutoff of 1.11 composite cortical standard uptake value ratio (SUVR) using the whole cerebellum as a reference region [1]. The final sample consisted of 90 participants: 20 CN-, nine CN+, 21 patients with eMCI+, 18 patients with lMCI+ and 22 patients with AD+. See demographic information on Table 1. Detailed inclusion criteria for the clinical diagnosis of the sample can be found at the ADNI website (<http://adni.loni.usc.edu/methods/>).

Imaging data acquisition:

MRI data were acquired on several 3T MRI scanners using scanner specific T1-weighted sagittal 3D MPRAGE and gradient echo EPI sequences. AV-45-PET were acquired on multiple scanners using scanners-specific acquisition protocols. In order to increase signal uniformity across the multicentre scanner platforms, original MPRAGE acquisitions and PET data in ADNI underwent standardized image pre-processing correction steps (<http://adni.loni.usc.edu/data-samples/>). A detailed description of the MRI and PET acquisition protocol can be found at the ADNI website (<http://adni.loni.usc.edu/data-samples/>).

Searchlight approach:

Searchlight approaches [2] are multivariate analysis methods that go through all voxels of interest in sequence (in this case, the selected voxels of the network) and examine voxel values in a ‘searchlight’ region of interest surrounding the current voxel. The measure of interest (in our case the correlation value) is then recorded in that voxel, resulting in a spatial map of local correlation measures. For this specific analysis we were interested in local correspondence between AV-45-uptake and iFC z-values that was not already accounted for by the global positive correlation $r_{\text{GLOBAL}}(\text{A}\beta, \text{iFC})$. Therefore, we first decorrelated voxel-wise AV-45-SUVr and iFC z-values across the whole network via Gram-Schmidt orthogonalization, ensuring a network

correlation of 0 between iFC and AV-45 uptake for each individual [3]. Then, for each voxel in the network, all voxels in its direct neighborhood (i.e., a sphere with a radius of 6 mm including ca. 100 voxels) were identified.

Control for grey matter atrophy:

In order to evaluate the influence of grey matter atrophy on the measures of local and global correspondence, grey matter atrophy was assessed using voxel-based morphometry. In order to be consistent with the threshold applied in the multimodal analysis, only voxels with a grey matter threshold above 0.5 were considered. An ANOVA model implemented in SPM8 (<http://www.fil.ion.ucl.ac.uk/spm/>) ($p < 0.001$ uncorrected) was used to assess grey matter atrophy once within a one-sample t-test mask over all subjects of the pDMN, once within the r_{LOCAL} ($A\beta$, iFC) cluster (see Figure 2 panel B). The main effect of group clusters derived from such ANOVA analyses were used to derive average levels of grey matter, once within regions atrophied within the whole pDMN, once within regions atrophied in the r_{LOCAL} ($A\beta$, iFC) cluster. Over all subjects, we used Pearson's correlation to associate averaged levels of grey matter within the pDMN atrophy cluster to r_{GLOBAL} ($A\beta$, iFC). Moreover, from the r_{LOCAL} ($A\beta$, iFC) cluster we derived averaged levels of grey matter and averaged levels of r_{LOCAL} ($A\beta$, iFC) for all subjects, that were associated to

each other via Pearson's correlation analysis. In order to assess regional specificity, the grey matter atrophy clusters derived from the previously mentioned ANOVA analyses were once overlaid on a one-sample t-test mask of the whole pDMN, once within the r_{LOCAL} ($A\beta$, iFC) cluster.

Supplementary Results:

Increased A β load and decreased iFC within the pDMN along the AD spectrum:

All analyses were performed within individually thresholded maps of the pDMN. Only voxels with z-values ≥ 1 and gray matter probability values ≥ 0.5 were included into the analyses. See Figure S1A to estimate the spatial extent of the thresholded pDMN (one-sample t-test over all subjects, $p < 0.05$). Investigating A β load within the pDMN revealed a main effect of group on AV-45 uptake (Figure S1B, ANOVA, $F=6.74$, $p<0.05$). Post-hoc t-tests revealed that group differences in AV-45 uptake were essentially between A β negative against A β positive subjects, with AV-45 uptake reaching a plateau already in CN+. Investigating iFC of the pDMN revealed a trend to significant main effect of group on iFC z-scores (Figure S1C, ANOVA, $F=2.10$, $p=0.09$). Post-hoc t-tests revealed a progressive decrease in pDMN iFC from CN- and eMCI+ over lMCI+ to AD+.

Grey matter atrophy is not associated with r_{GLOBAL} (A β , iFC) and r_{LOCAL} (A β , iFC):

Voxel-based morphometry analyses within the whole pDMN revealed modest grey matter group differences in the cerebellum ($p<0.001$ uncorrected), showing little overlap with core brain regions of the pDMN as the posterior cingulate and precuneus

(Figure S2A). Over all participants, averaged grey matter values derived from the atrophy cluster did not significantly correlate with averaged iFC z-values of the pDMN (Figure S2B, $R = -0.06$, $p=0.45$). Voxel-based morphometry analyses within the r_{LOCAL} ($A\beta$, iFC) cluster (see Figure 2B) revealed spurious group differences for grey matter in few voxels of medial posterior parietal areas of the pDMN (Figure S2C, $p<0.001$ uncorrected). Over all participants, averaged grey matter values derived from the atrophy cluster did not significantly correlate with averaged r_{LOCAL} ($A\beta$, iFC) (Figure S2D, $R = -0.13$, $p=0.20$).

Supplementary References:

- [1] Fleisher a. S, Chen K, Liu X, Roontiva a., Thiyyagura P, Ayutyanont N, Joshi a. D, Clark CM, Mintun M a., Pontecorvo MJ, Doraiswamy PM, Johnson K a., Skovronsky DM, Reiman EM (2011) Using Positron Emission Tomography and Florbetapir F 18 to Image Cortical Amyloid in Patients With Mild Cognitive Impairment or Dementia Due to Alzheimer Disease. *Arch Neurol* **68**, 1404–1411.
- [2] Myers N, Pasquini L, Göttler J, Grimmer T, Koch K, Ortner M, Neitzel J, Mühlau M, Förster S, Kurz A, Förstl H, Zimmer C, Wohlschläger AM, Riedl V, Drzezga A, Sorg C

(2014) Within-patient correspondence of amyloid- β and intrinsic network connectivity in Alzheimer's disease. *Brain* **137**, 2052–2064.

- [3] Kriegeskorte N, Goebel R, Bandettini P (2006) Information-based functional brain mapping. *Proc Natl Acad Sci U S A* **103**, 3863–3868.

Supplementary Legends

Figure S1. Increased AV-45 uptake and decreased pDMN iFC

z-values across the AD spectrum. (A) Spatial extent of the thresholded pDMN used in the study; the pDMN mask was identified by independent component analysis of fMRI data, automated component selection based on pDMN template, and one-sample t-test over iFC z-maps of all subjects ($p < 0.05$). Only voxels with z-values ≥ 1 and gray matter probability values ≥ 0.5 were included into the analyses. (B) Group differences in mean AV-45 uptake within the pDMN (ANOVA and related post-hoc t-tests, $p < 0.05$). (C) Group differences in mean iFC z-values differences within the pDMN (ANOVA and related post-hoc t-tests, $p < 0.05$). AD = Alzheimer's disease; AD+ = A β positive AD; a.u. = arbitrary units; pDMN = posterior default mode network; eMCI+ = A β positive early mild cognitive impairment; iFC = intrinsic functional connectivity; lMCI+ = A β positive late mild cognitive impairment; CN- = A β negative cognitively normal subjects; CN+ = A β positive cognitively normal subjects; SUVR = standardized uptake value ratio.

Figure S2. Global and local correspondence are not

substantially affected by atrophy. (A) Voxel-based morphometry analyses reduced to a one-sample t-test mask over all subjects of

the pDMN (in red), reveals group differences in grey matter within the cerebellum (green). (B) Averaged levels of grey matter derived from the atrophy cluster in the pDMN do not significantly correlate with averaged r_{GLOBAL} ($A\beta$, iFC) within the pDMN (Pearson's correlation coefficient, $p < 0.05$, all participants included). (C) Voxel-based morphometry analyses reduced to the r_{LOCAL} ($A\beta$, iFC) cluster (in red, see also Figure 2B), reveals spurious group differences in grey matter in few voxels located within medial posterior areas of the pDMN (green). (D) Within the r_{LOCAL} ($A\beta$, iFC) cluster, averaged levels of grey matter derived from the atrophy cluster do not significantly correlate with averaged r_{LOCAL} ($A\beta$, iFC) levels (Pearson's correlation coefficient, $p < 0.05$, all participants included). A.u. = arbitrary units; GM = grey matter; iFC = intrinsic functional connectivity; pDMN = posterior default mode network.

Supplementary Figures:

Figure S1:

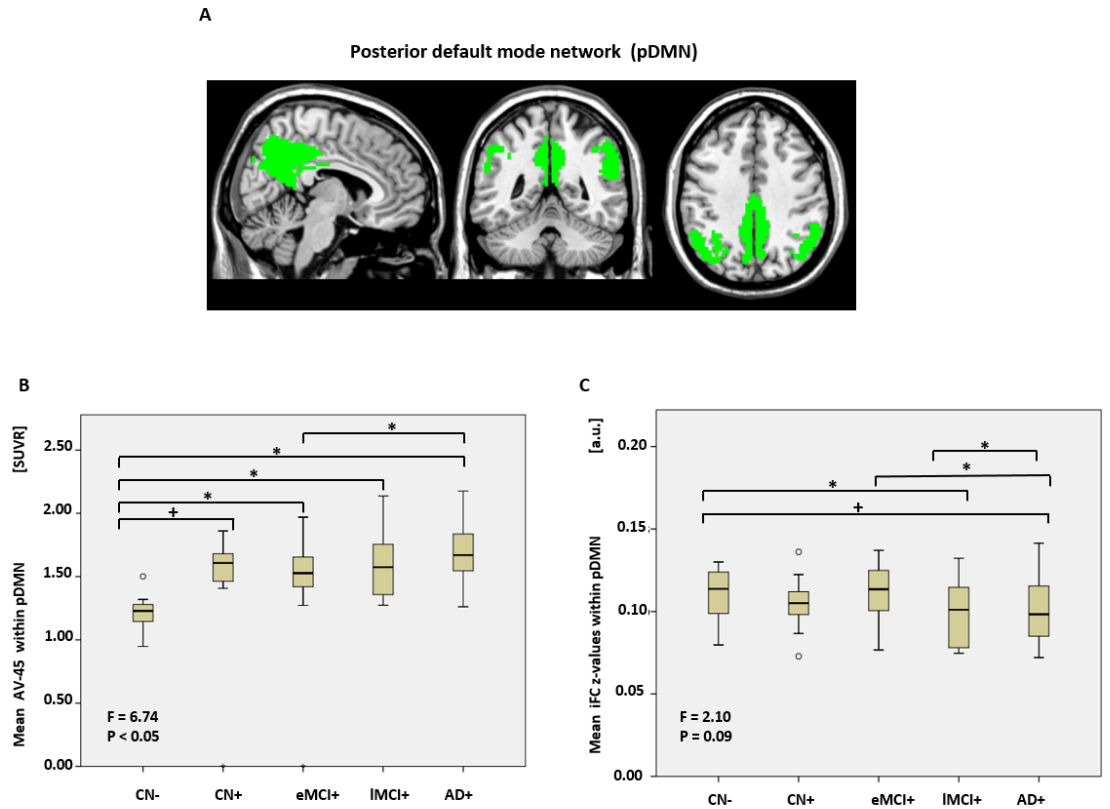


Figure S2:

